Chemical Engineering Journal 164 (2010) 418–424

Contents lists available at ScienceDirect

Chemical Engineering Journal

journal homepage: www.elsevier.com/locate/cej

Fluid dynamics simulation of the high shear mixing process

Anders Darelius[a,1], Johan Remmelgas[c], Anders Rasmuson[a,*], Berend van Wachem[b], Ingela Niklasson Björn[c]

[a] Department of Chemical and Biological Engineering, Chalmers University of Technology, SE-412 96 Göteborg, Sweden
[b] The Department of Mechanical Engineering, Imperial College London, Exhibition Road, London SW7 2AZ, United Kingdom
[c] AstraZeneca Centre of Excellence for Process Analytical Technology, R&D Mölndal, SE-431 83 Mölndal, Sweden

ARTICLE INFO

Article history:
Received 7 July 2009
Received in revised form 6 December 2009
Accepted 14 December 2009

Keywords:
Fluid mechanics
Kinetic theory of granular flow
Frictional stress models
Powder technology
Granulation
Multiphase flow

ABSTRACT

The Eulerian–Eulerian two-fluid approach for modelling multiphase flows is used to simulate the flow in a high shear mixer. The results are compared with experimental velocity profiles for the solids phase at the wall in the mixer obtained using a high speed camera (Darelius et al. Chem. Eng. Sci. 62 (2007) 2366).

The governing equations are closed using relations from the Kinetic Theory of Granular Flow (KTGF) combined with a frictional stress model due to Johnson and Jackson and Schaeffer and inter-phase drag due to Wen and Yu. In addition, calculations are presented for a model with a constant particle phase viscosity (CPV). Free slip and partial slip boundary conditions for the solid phase velocity at the vessel wall and the impeller have been utilized.

The results show that the bed height could be well predicted by the partial slip model, whereas the free slip model could not capture the experimentally found bed height satisfactorily. For the KTGF model, the swirling motion of the rotating torus that is formed by the moving powder bed was over-predicted and the tangential wall velocity was under-predicted, probably due to the fact that the frictional stress model needs to be further developed, e.g. to tackle cohesive particles in dense flow. The CPV model gave predictions in good agreement with the experiments for a solids viscosity of 0.1 Pa s and a wall slip parameter of 0.005 m/Pa s. However, for a very low or very high value of the particle phase viscosity and for a high value of the wall slip parameter the agreement with experiments was poor. Interestingly, values of the viscosity that are commonly employed for fluidized beds seem applicable also in the present case.

1. Introduction

Granulation in high shear mixers is an important unit operation often used in the development and manufacturing of tablets in the pharmaceutical industry. The process comprises a dry mixing step, where the active substances and excipients are mixed together in order to form a homogeneous mixture, followed by a wet mixing step, where binder liquid is added in order to build up agglomerates. Many researchers have focused on agglomeration and breakage mechanisms in the high shear mixer, e.g. Iveson et al. [1] and Reynolds et al. [2]. However, a better understanding of the local mixing and the flow pattern in the granulator is necessary in order to implement the agglomeration and breakage models and to develop quantitative process models that enable predictive scale-up and process optimization. This is highlighted by several authors, e.g. Cameron et al. [3], Faure et al. [4] and Niklasson Björn et al. [5].

The aim of this study is to obtain a quantitative understanding of the flow behaviour of particles in a high shear mixer via fluid mechanics calculations based upon the two-fluid model. The calculated results are compared to the experimental data obtained by Darelius et al. [8] using a high speed camera. In the simulation of fluidized beds, the kinetic theory of granular flow (KTGF), where colliding particles are treated in a similar fashion to colliding molecules in an ideal gas, has been shown to be a promising model for modelling particle–particle interactions (see e.g. van Wachem et al. [6]) and this model is therefore employed here as well. However, for the present flow it is expected that particles will be in sustained contact to a greater extent than in a fluidized bed so that the stresses between particles becomes larger than what is predicted by KTGF. Thus, a frictional stress model is used in combination with KTGF.

2. Mathematical model

2.1. The Eulerian–Eulerian approach

In the Eulerian–Eulerian two-fluid approach for modelling multiphase flows, the fluid and dispersed phases are averaged over a

* Corresponding author. Tel.: +46 31 7722940; fax: +46 31 7723035.
E-mail address: rasmuson@chalmers.se (A. Rasmuson).
[1] Present address: Epsilon Utvecklingscentrum Väst, Lindholmspiren 9, SE-417 56 Göteborg, Sweden.

1385-8947/$ – see front matter © 2009 Elsevier B.V. All rights reserved.
doi:10.1016/j.cej.2009.12.020

fixed volume that is large in comparison with the size of the individual particles. The conservation equations for momentum and mass for the gas phase in a gas–solid flow can be written as (Anderson and Jackson [9])

$$\frac{\partial(\alpha_g\rho_g\mathbf{u}_g)}{\partial t} + \nabla\cdot(\alpha_g\rho_g\mathbf{u}_g\mathbf{u}_g) = -\alpha_g\nabla P + \nabla\cdot\left(\alpha_g\overline{\overline{\tau_g}}\right) - \beta(\mathbf{u}_g-\mathbf{u}_s)+\mathbf{F} \quad (1)$$

$$\frac{\partial(\alpha_g\rho_g)}{\partial t} + \nabla\cdot(\alpha_g\rho_g\mathbf{u}_g) = 0 \quad (2)$$

where α_g is the volume fraction of the gas, ρ_g is the gas density, $\mathbf{u}_g$ is the gas velocity, P is the pressure, $\overline{\overline{\tau_g}}$ is the viscous stress tensor for the gas phase, β is the inter-phase momentum exchange coefficient, $\mathbf{u}_s$ is the solid phase velocity and $\mathbf{F}$ represents all external forces acting on the system. For the solid phase, the corresponding equations are expressed as

$$\frac{\partial(\alpha_s\rho_s\mathbf{u}_s)}{\partial t} + \nabla\cdot(\alpha_s\rho_s\mathbf{u}_s\mathbf{u}_s) = -\alpha_s\nabla P - \nabla P_s + \nabla\cdot\left(\alpha_s\overline{\overline{\tau_s}}\right) + \beta(\mathbf{u}_g-\mathbf{u}_s)+\mathbf{F} \quad (3)$$

$$\frac{\partial(\alpha_s\rho_s)}{\partial t} + \nabla\cdot(\alpha_s\rho_s\mathbf{u}_s) = 0 \quad (4)$$

where α_s is the volume fraction of the particle phase, ρ_g is the density of the particles, τ_s is the particle phase viscous stress tensor, and P_s is the solids pressure. The volume fractions sum to unity, i.e.

$$\sum_{k=1}^{n}\alpha_k = 1 \quad (5)$$

For both phases, the viscous stress tensor is described by Newton's law of viscosity as

$$\overline{\overline{\tau_k}} = \left(\lambda_k - \frac{2}{3}\mu_k\right)(\nabla\cdot\mathbf{u}_k)\bar{\bar{I}} + 2\mu_k\overline{\overline{S_k}} \quad (6)$$

where λ_k is the bulk viscosity, μ_k is the dynamic viscosity and $\overline{\overline{S_k}}$ is the strain rate tensor for phase k. The strain rate tensor describes the deformation of a fluid element and is defined as

$$\overline{\overline{S_k}} = \frac{1}{2}\left(\nabla\mathbf{u}_k + (\nabla\mathbf{u}_k)^T\right) \quad (7)$$

The bulk viscosity of a fluid is a measure of the difference between the thermodynamic and mechanical pressures.

For the gas phase, the dynamic viscosity is assumed to be 1.789×10^{-5} Pa s while the bulk viscosity is set to zero in what is referred to as the Stokes' assumption. For the solids phase, the dynamic and bulk viscosities are modelled using either the kinetic theory of granular flow (KTGF Model) as described by Darelius et al. [17] or using a model with a constant particle phase viscosity (CPV Model). In the former case, the total shear viscosity is the sum of the viscosity calculated based upon the kinetic theory of granular flow and a frictional viscosity, as described below.

2.2. Inter-phase momentum exchange

Several models describing the inter-phase momentum exchange exist in the literature. van Wachem et al. [6] have compared different models and shown that the Wen and Yu [10] model performs well over the range of relevant solid volume fractions. The model for the exchange coefficient is formulated as

$$\beta = \frac{3}{4}C_D\frac{(1-\alpha_s)\alpha_s\rho_g\left|\mathbf{u}_g-\mathbf{u}_s\right|}{D_p}(1-\alpha_s)^{-2.65} \quad (8)$$

where D_p is the particle diameter and C_D is the drag coefficient for a single sphere (Rowe [11]):

$$C_D = \begin{cases} 24\dfrac{(1+0.15((1-\alpha_s)Re_p)^{0.687})}{Re_p(1-\alpha_s)} & \text{if } Re_p(1-\alpha_p) < 1000 \\ 0.44 & \text{if } Re_p(1-\alpha_p) \geq 1000 \end{cases} \quad (9)$$

The particle Reynolds' number is defined as

$$Re_p = \frac{D_p\rho_g\left|\mathbf{u}_g-\mathbf{u}_s\right|}{\mu_g} \quad (10)$$

2.3. Closures

Further modelling is needed to provide closures for the particle momentum equations in terms of the solids pressure and the solids phase viscosity. It has been shown by van Wachem et al. [6] that the kinetic theory of granular flow (KTGF), in conjunction with a frictional stress model, works well for moderate to dense gas–particle flows. The KTGF model is an extension of the model for molecular motion in a dense gas that takes into account non-ideal particle–particle interactions (Chapman and Cowling [12]). Numerous studies on KTGF have been published; a detailed derivation is given by, e.g. Gidaspow [13] or Peirano and Leckner [14]. The KTGF model assumes particle–particle interactions to be binary and instantaneous. However, at a high solids volume fraction sustained particle–particle contacts occur, resulting in much higher particle stresses. Hence, an additional frictional contribution must be added to the solids pressure and dynamic solids viscosity. These extra contributions constitute parts of the modelling framework known as frictional stress models, which are used frequently in, e.g. the field of soil mechanics to model avalanches, landslides, etc.

In this work, the extra solid particle pressure, i.e. the frictional pressure, is modelled using the semi-empirical model proposed by Johnson and Jackson [15], namely:

$$P_f = Fr\frac{(\alpha_s-\alpha_{s,\min})^n}{(\alpha_{s,\max}-\alpha_s)^q} \quad (11)$$

where $\alpha_{s,\min}$ is the minimum volume fraction above which frictional forces are important, and Fr, n, and q are empirical constants. The frictional dynamic viscosity that is added to the solid dynamic viscosity is related to P_f through the linear law in an expression derived by Schaeffer [16]:

$$\mu_f = \frac{P_f\sin\varphi}{2\sqrt{I_{2D}}} \quad (12)$$

where φ is the angle of internal friction and I_{2D} is the second invariant of the strain rate tensor $\overline{\overline{S_s}}$ (Eq. (7)). It should be noted that this expression is valid for cohesion-less materials only and it is expected that cohesion will even further increase the particle–particle stresses. Further details are provided by Darelius et al. [17].

Calculations are also carried out also for a model with constant particle viscosity (CPV) in which the solids pressure is modelled using the expression due to Bouillard et al. [24]. For this latter model a compaction modulus of 20 and a reference modulus of elasticity of 1 Pa is assumed based upon previous studies of fluidized beds.

2.4. Boundary conditions

The continuous phase (air) is assumed to obey the no slip boundary condition at the wall and on the impeller. The word wall includes both vessel walls and the impeller hereinafter. For the solid phase, different boundary conditions can be found in the literature. Free slip is used by numerous authors for modelling the solid phase wall velocity in fluidized beds, e.g. van Wachem et al. [6]. Johansson

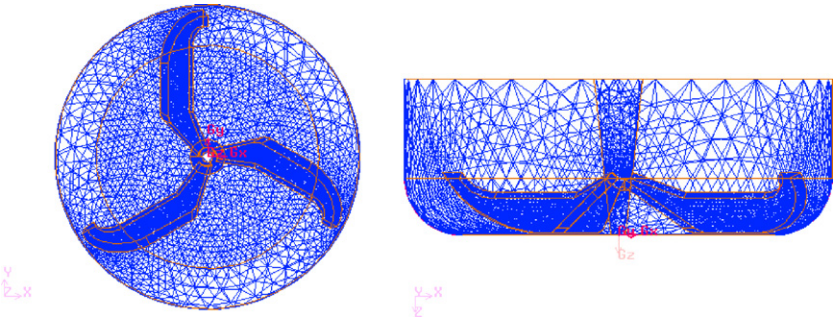

Fig. 1. Computational mesh in the impeller region.

[18] has used partial slip for the particles at the wall in a fluidized bed using a model proposed by Eldighidy et al. [19]. The present work employs a partial slip model based on Tu and Fletcher [20] which is a combination of no slip and free slip, covering the whole range in between these two extremes. The expression is

$$a\varphi_w - b\left.\frac{\partial\varphi}{\partial\eta}\right|_w = 0 \tag{13}$$

where φ_W is the tangential solid velocity at the wall, η is the normal direction of the wall directed into the flow regime and a and b are positive constants. According to Tu and Fletcher [20] the constants a and b are functions of the coefficients of wall restitution and the ratio a/b is a measure of the degree of slip. In the tangential direction an infinite ratio corresponds to no slip and a zero ratio represents free slip.

For the CPV model, the partial slip is expressed with Eq. (13) with $\phi = u_w$, $a = 1$ and b given by

$$b = \psi\mu_s \tag{14}$$

where μ_s is the solids phase viscosity and ψ is a parameter referred to as the wall slip parameter.

3. Simulations

3.1. The high shear system studied

The system considered is a MiPro high shear mixer (ProCept, Belgium) with an inner diameter of 150 mm, a volume of 1900 ml and a three-bladed bevelled impeller. To be able to compare the simulated results with experimental data, the simulated powder was assumed to be mono-disperse and to have properties similar to coarse microcrystalline cellulose (MCC) with particle diameter of 59 μm. Owing to symmetry, it would be possible to model only a third of the tank (a three-bladed impeller), but larger structures of the flow, as described, e.g. by Kilander and Rasmuson [21], would then not necessarily be detected.

3.2. Solution strategy and convergence

3.2.1. KTGF model

The mesh was constructed in Gambit version 2.3.16 (Ansys Inc., US) and the impeller geometry was based on an imported CAD drawing of the original impeller. The mesh contains 160,000 cells, hexahedral cells in the upper zone and tetrahedrons in the zone close to the impeller (Fig. 1). Calculations were carried out for cases with a sliding mesh interface between the upper and lower zones as well as for cases where both zones were rotating.

The impeller speed was set at 450 rpm. The chopper was not modelled. In total, four simulations were run, employing three different boundary conditions for the solid phase. The first three simulations used the sliding mesh approach. In the first simulation, the free slip wall boundary condition was employed. In the second and third simulations, the partial slip condition was used with the coefficients of wall restitution set to $e_p^N = e_p^T = 0.5$ and 0.95, respectively. Finally, in the last simulation, there was no sliding mesh interface and the partial slip condition with $e_p^N = e_p^T = 0.5$ was employed (as in the second simulation). Since the physical interpretation of the coefficients of restitution might not be meaningful for dense systems they are to be treated as empirical adjustable parameters.

Fluent 6.3.26 (Ansys Inc., US) was used for the simulation. Material properties, discretization schemes and convergence criteria used are discussed in Darelius et al. [17]. A time step of 0.74 ms corresponding to a 2° impeller rotation was used for the simulation except at start up where a shorter step was utilized. Weak convergence behaviour was shown and hence, approximately 100 iterations per time step were necessary throughout the simulation.

3.2.2. CPV model

Additional calculations using CFX (version 11.0) were employed to further study the effects of spatial discretization, wall boundary conditions and particulate viscosity using a model with 146,000 tetrahedral cells. In this latter case, the clearance between the tip of the impeller and the vessel wall and bottom was neglected and only one third of the geometry was modelled. Lastly, a wall rather than a pressure boundary was used at the top of the vessel. The CFX calculations were carried out using a time step corresponding to an impeller rotation of between 0.5° and 1.4°. Initial transients were allowed to decay for the first 15 impeller revolutions and time-averaged quantities were then calculated based upon an averaging period of 7.5 revolutions.

4. Experimental

The experiments were performed in the MiPro equipment described in the previous section. MCC (Avicel PH102 special grade, FMC Biopolymer) with a number average diameter of 59 μm was used. A high speed camera with a capacity of 2000 frames per second was used to measure the surface velocities of the MCC powder at the wall of the transparent glass vessel. The experimental procedure is described in detail by Darelius et al. [8]. Laser Doppler Anemometry (LDA) measurements were also performed but are not used here [7].

5. Results and discussion

5.1. KTGF model

After approximately 50 simulated impeller revolutions, a stable slowly pulsating bed behaviour was observed. This could be observed as a slow fluctuation in the volume fraction and powder velocity. The frequency of the pulsations corresponded to approx-

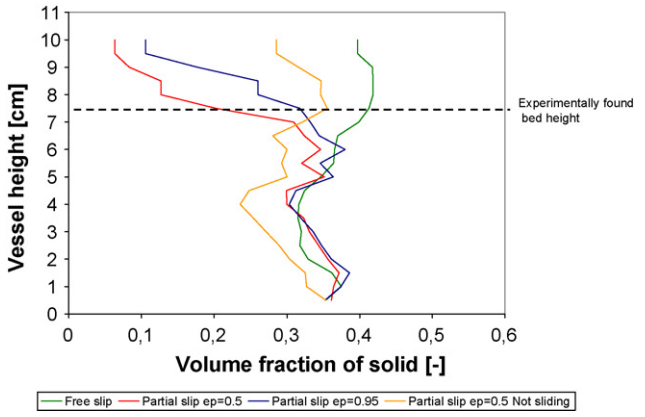

Fig. 2. Simulated volume fractions at the wall at different bed heights. The dotted line is the experimentally found average bed height.

imately two impeller revolutions and was considered to represent low frequency macro-instabilities, such as the ones described by Kilander and Rasmuson [21] for mixing of liquids in square tanks. Fig. 2 shows the simulated average volume fraction of solid along the wall for the four simulations performed. The averaged simulated values were obtained by averaging the volume fractions in all computational cells next to the wall at specific vessel heights.

Experimentally, it was found that the average height of the pulsating bed was roughly 7.5 cm from the bottom and the pulsating variation was estimated to be ±1 cm. The average experimental bed height is shown as a dotted line in Fig. 2. When comparing the simulations to the observation, it is clear that the bed height is better predicted when the partial slip condition is utilized instead of the free slip condition. In the latter case, the decrease in volume fraction towards the top of the vessel is not captured at all. However, from the results of the simulations with/without sliding mesh, it is clear that the slowly fluctuating macro-instabilities affect the result. The volume distributions in the two simulations differ, indicating different positions in the macro-instability cycle. That is, there is a difference in the results calculated by the two different models because the results are not compared at exactly the same point in time.

The volume fraction distribution in the entire granulator can be used as an indication of how important the frictional stresses are in comparison with the stress contribution from KTGF. In Fig. 3, a histogram of the overall volume fraction distribution is shown. It can be seen that a non-negligible part of the vessel has a volume fraction larger than $\alpha_{s,\min}$ (=0.5) which means that the frictional contribution to the stresses has to be taken into account in these regions. The dense regions with $\alpha_{s,\min} > 0.5$ are mainly present in

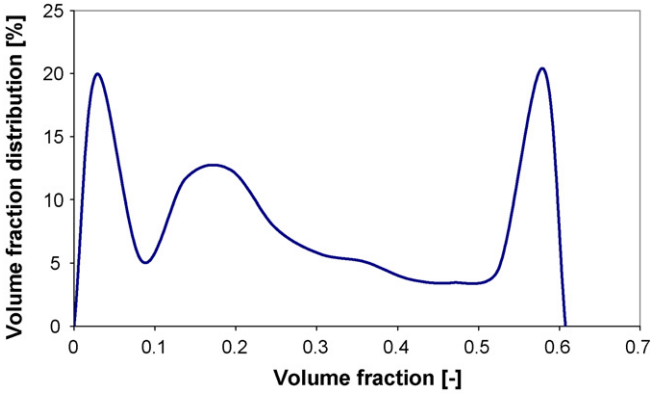

Fig. 3. Histogram over the volume fraction distribution in the vessel.

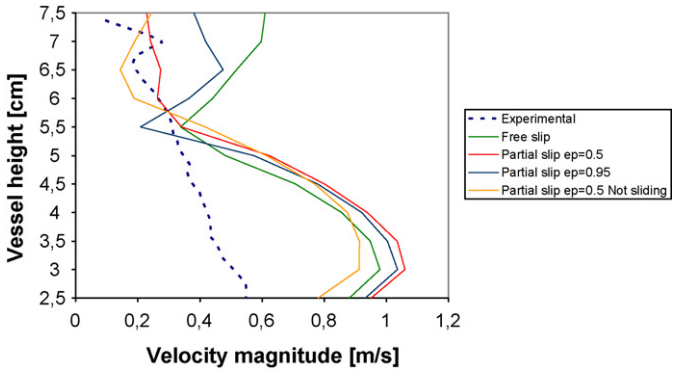

Fig. 4. Comparison between wall velocity magnitudes obtained from experiments and simulations.

front and right above the impeller blades where the material is subject to major momentum transfer from the impeller blades.

Fig. 4 shows the experimental and simulated averaged velocity magnitude at the vessel wall. For both the free and partial slip simulations, the velocity levels are reasonably well predicted when considering that the model is based upon assumptions of monodisperse and cohesion-less interacting particles that might not be relevant for dense systems where frictional stresses are important. In the experiments, the velocity magnitude reaches its maximum at the top of the impeller and then decreases approximately linearly with distance further up along the wall, except near a height of 7 cm where there is a local maximum in the velocity. In the simulations the velocity maximum is reached slightly above the impeller tip and the velocity decreases faster when going up along the vessel wall to a height of approximately 5.5 cm. The maximum velocity magnitude is over-predicted for all simulations and the velocity difference between simulations with/without sliding mesh is again due to macro-instabilities as explained for the volume fraction in Fig. 2.

However, when splitting the wall velocity into its tangential and axial components, as is done in Figs. 5 and 6, it becomes obvious that the magnitude of the tangential wall velocity component is under-predicted whereas the magnitude of the axial wall velocity is over-predicted at least in the lower part of the vessel. However, as can be seen in Figs. 5 and 6, the magnitude of the axial velocity at the wall is greater than the magnitude of the tangential velocity at the wall in the simulations. One possible explanation for the simulated redistribution of tangential and axial momentum is that in the dense particle region, the fluid description of the solid material fails to capture frictional effects that are important when the powder is deflected by the impeller blade as briefly mentioned by Knight et al. [22]. Other possible reasons for the poor agreement

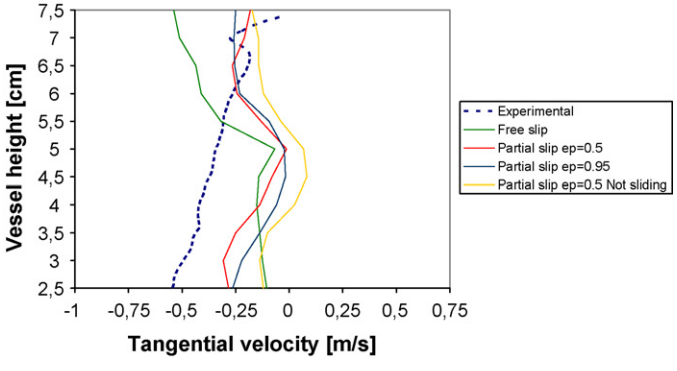

Fig. 5. Comparison between averaged tangential velocity profiles obtained from experiments and simulations.

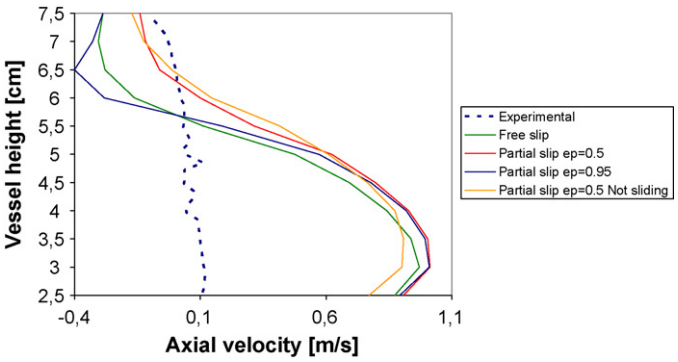

Fig. 6. Comparison between averaged axial velocity profiles obtained from experiments and simulations.

with experiments may be that cohesive forces are neglected in the impeller region or that the mesh size is too coarse in the vicinity of the impeller and needs to be refined in order to resolve the large gradients present in this region.

Fig. 5 shows the measured averaged tangential velocity profile together with corresponding simulated profiles. Negative tangential velocity indicates clockwise tangential flow in the vessel. As can be seen, the simulation using the free slip boundary condition for the solids phase under-predicts the wall velocity in the lower region of the vessel, whereas over-prediction occurs in the top region. For the partial slip model, better agreement with the experimental data is obtained in the upper region even though under-prediction still occurs when approaching the dense region close to the impeller.

The corresponding axial velocity distribution is displayed in Fig. 6. Positive axial velocity indicates upward flow along the vessel wall, which is typical for the secondary swirling motion of a rotating torus in the roping regime in a high shear mixer (Litster et al. [23]). However, the swirling motion is over-predicted in the simulation, especially in the lower vessel region where the largest velocity gradients are present.

The overall result when introducing partial slip instead of free slip is that the energy dissipation at the wall increases, resulting in slightly better prediction of the bed height and slightly improved prediction of the powder velocity as well. There is no obvious difference between the results obtained for the different coefficients of restitution used in the partial slip model. This highlights the need for further development of partial slip models.

5.2. CPV model

The calculations using the CPV model may also be compared to the experimental data. Figs. 7 through 12 show the tangential and axial velocities at the wall for different values of the solid viscosity and wall slip parameter. For a small value of the wall slip parameter and solids shear viscosities of 0.1 Pa s or 1 Pa s the agreement between the experimental data and the calculated result is quite reasonable. However, for very small and large values shear viscosity (0.01 Pa s and 10 Pa s, respectively) and for large values of the wall slip parameter the agreement is poor. Although there may be considerable error in the experimental data, it is interesting to note that there is qualitative as well as quantitative agreement between the experimental data and the model predictions. That is, both the experiment and the calculations indicate that there is a local maximum in the magnitude of the averaged tangential velocity towards the top of the vessel. The comparison with the experimental data indicate that the solids shear viscosity should be in the neighborhood of 0.1 Pa s, which is also the viscosity that typically is used for fluidized bed calculations. As to the wall slip parameter, Figs. 7 through 12

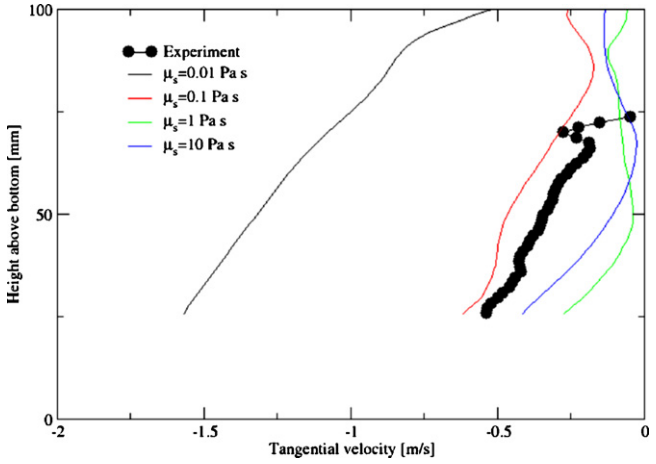

Fig. 7. The time-averaged tangential solids velocity at the wall for a wall slip parameter 0.005 m/Pa s and different values of the solids viscosities.

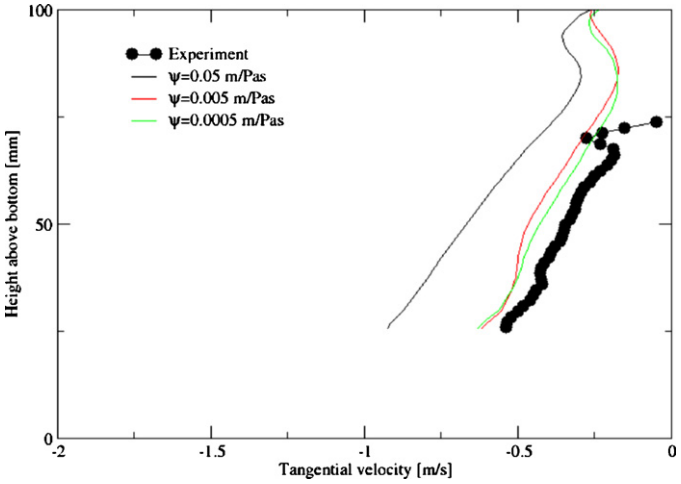

Fig. 8. The time-averaged tangential solids velocity at the wall for a solids viscosity of 0.1 Pa s and different values of the wall slip parameter.

indicate that a value smaller than 0.05 m/Pa s may be appropriate.

There are two notable differences between the present CPV and KTGF models. Firstly, the KTGF model predicts a shear viscosity

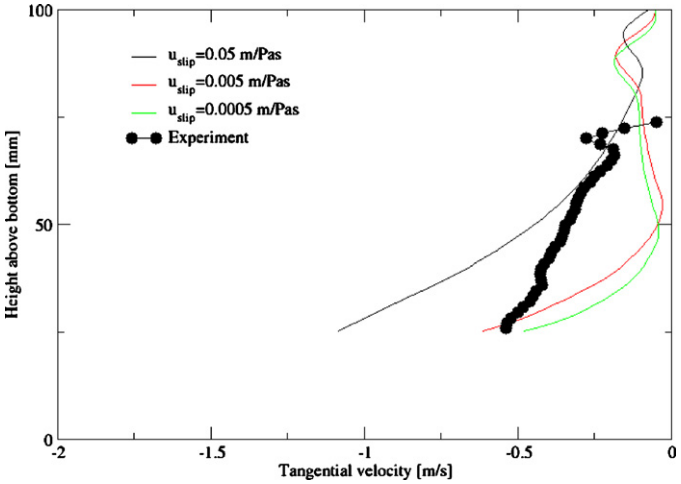

Fig. 9. The time-averaged tangential solids velocity at the wall for a solids viscosity of 1.0 Pa s and different values of the wall slip parameter.

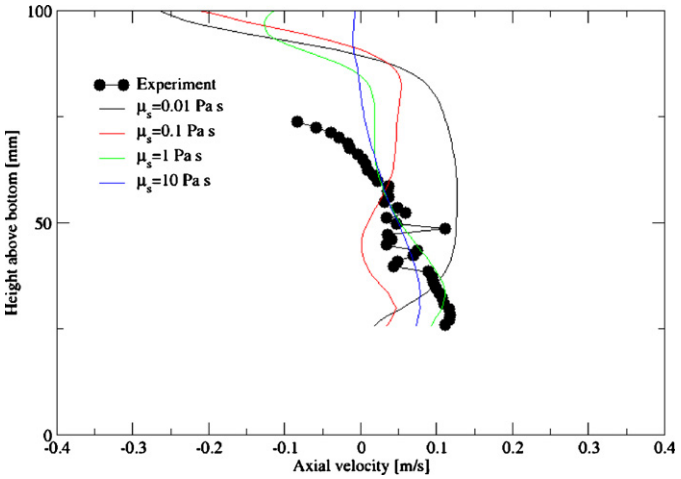

Fig. 10. The time-averaged axial solids velocity at the wall for a wall slip parameter 0.005 m/Pa s and different values of the solids viscosities.

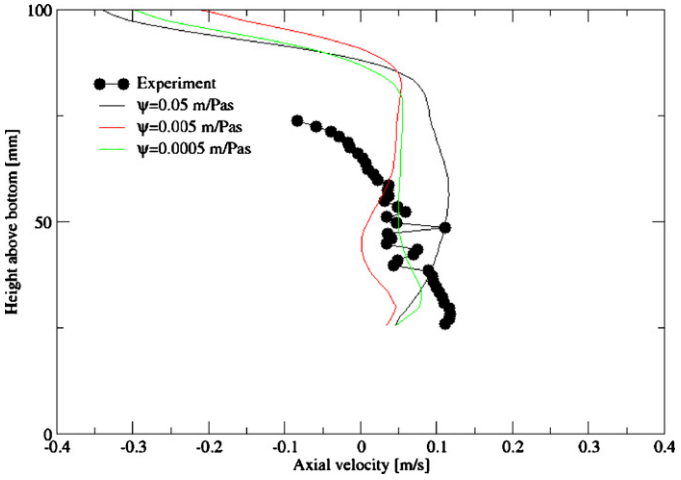

Fig. 11. The time-averaged axial solids velocity at the wall for a solids viscosity of 0.1 Pa s and different values of the wall slip parameter.

that is much lower than the viscosity employed in the CPV model. Secondly, the CPV model does not include any frictional stress contribution. It may therefore be that the CPV model is successful in predicting the experimentally observed behaviour because the

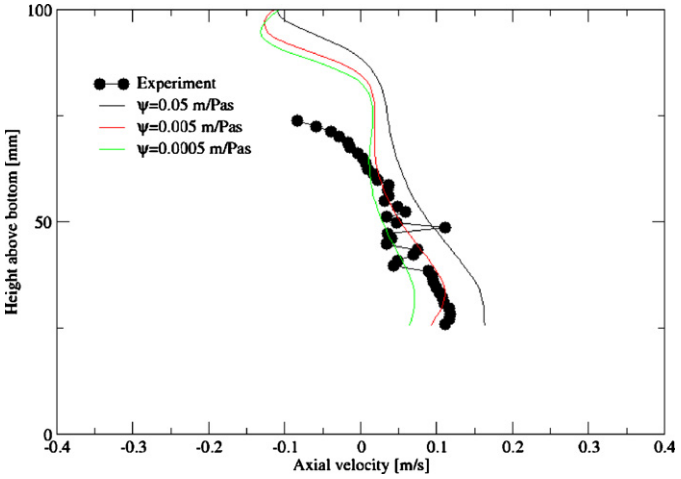

Fig. 12. The time-averaged axial solids velocity at the wall for a solids viscosity of 1.0 Pa s and different values of the wall slip parameter.

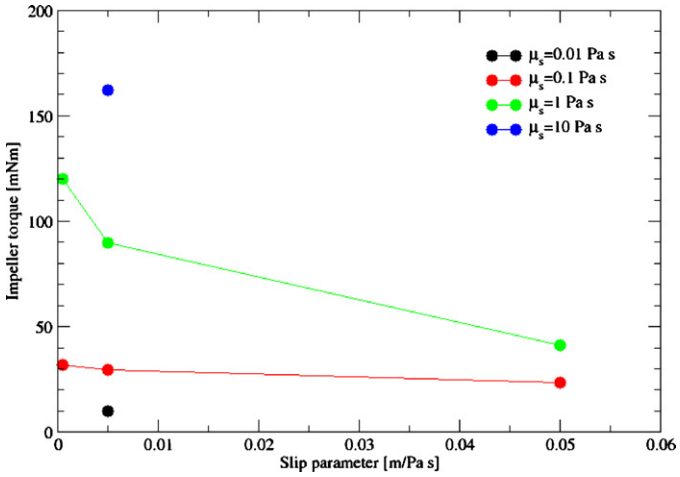

Fig. 13. The steady-state impeller torque as a function of the slip parameter for different values of the solids viscosity.

large value of the shear viscosity in the CPV model compensates for its lack of frictional stress. Presumably, the present KTGF model would also give predictions in agreement with experiments if the frictional stress model was improved upon.

Lastly, the predicted impeller torque and its dependence on the solids viscosity and the wall slip parameter are examined for the CPV model. Fig. 13 shows the steady-state impeller torque as a function of the wall slip parameter for different values of the solids viscosity. The predicted impeller torque increases as the solids viscosity increases and as the wall slip parameter decreases, as expected. The torque is of interest because measurements of the torque are obtained in manufacturing and may possibly be employed for further comparison with calculations.

6. Conclusions

In this study, the Eulerian–Eulerian two-fluid approach to modelling multiphase flows was applied to the dense gas–solid flow in a high shear mixer. The Kinetic Theory of Granular Flow combined with frictional stress models was used to model the solids phase stress. Different boundary conditions for the solid phase at the vessel wall were used, i.e. the free and partial slip conditions. The partial slip condition that was implemented is a function of the coefficient of wall restitution for the particles and was derived for dilute particle systems by Tu and Fletcher [20].

Calculated results were compared to the experimental data obtained by Darelius et al. [8]. It was found that the bed height could not be captured in the simulations with the model based upon kinetic theory of granular flow using a free slip wall boundary condition for the solids phase. However, as partial slip was implemented to increase energy dissipation at the wall, the bed height was well predicted. Moreover, the wall velocity magnitude could be reasonably well predicted using both free and partial slip boundary conditions, but the prediction of the velocity direction was poor as too much particle tangential momentum was transformed into axial momentum at the vessel wall. There was no obvious difference between the simulated results using different coefficients of restitution (e_p = 0.5 and 0.95, respectively) in the partial slip model, which emphasises a need for developing partial slip models for dense systems with sustained particle-wall contact.

Additional calculations showed that by using a model with constant particle phase viscosity, good agreement with experimentally determined velocity at the wall could be obtained. In the present case, the calculated velocity profile was quantitatively and qualitative similar to the experimental velocity profiles for

a solids shear viscosity of 0.1 Pa s and a wall slip parameter of 0.005 m/Pa s. However, for values of the solids phase viscosity as small as 0.01 Pa s or as large as 10 Pa s and for large values of the wall slip parameter, the agreement between the calculated results was poor.

Acknowledgement

Financial support from AstraZeneca R&D, Mölndal, Sweden is gratefully acknowledged.

References

[1] S.M. Iveson, N.W. Page, J.D. Litster, The importance of wet-powder dynamic mechanical properties in understanding granulation, Powder Technology 130 (2003) 97–101.
[2] G.K. Reynolds, J.S. Fu, Y.S. Cheong, M.J. Hounslow, A.D. Salman, Breakage in granulation: a review, Chemical Engineering Science 60 (2005) 3969–3992.
[3] I.T. Cameron, F.Y. Wang, C.D. Immanuel, F. Stepanek, Process systems modelling and applications in granulation: a review, Chemical Engineering Science 60 (2005) 3723–3750.
[4] A. Faure, P. York, R.C. Rowe, Process control and scale-up of pharmaceutical wet granulation processes: a review, European Journal of Pharmaceutics and Biopharmaceutics 52 (2001) 269–277.
[5] I. Niklasson Björn, A. Jansson, M. Karlsson, S. Folestad, A. Rasmuson, Empirical to mechanistic modelling in high shear granulation, Chemical Engineering Science 60 (2005) 3795–3803.
[6] B.G.M. van Wachem, J.C. Schouten, C.M. van den Bleek, J.L. Sinclair, Comparative analysis of CFD models of dense gas–solid systems, AIChE Journal 47 (2001) 1035–1051.
[7] A. Darelius, A. Rasmuson, I. Niklasson Björn, S. Folestad, LDA measurements of near wall powder velocities in a high shear mixer, Chemical Engineering Science 62 (2007) 5770–5776.
[8] A. Darelius, E. Lennartsson, A. Rasmuson, I. Niklasson Björn, S. Folestad, Measurement of the velocity field and frictional properties of wet masses in a high shear mixer, Chemical Engineering Science 62 (2007) 2366–2374.
[9] T.B. Anderson, R. Jackson, A fluid mechanical description of fluidized beds, Industrial & Engineering Chemistry Fundamentals 6 (1967) 527–539.
[10] C.Y. Wen, Y.H. Yu, Mechanics of fluidization, Chemical Engineering Progress Symposium Series 62 (1966) 100–111.
[11] P.N. Rowe, Drag forces in a hydraulic model of a fluidized bed, part II, Transactions of the Institution of Chemical Engineers 32 (1961) 175–180.
[12] S. Chapman, T.G. Cowling, The Mathematical Theory of Non-uniform Gases, Cambridge University Press, 1970.
[13] D. Gidaspow, Multiphase Flow and Fluidization—Continuum and Kinetic Theory Descriptions, Academic Press, London, England, 1994.
[14] E. Peirano, B. Leckner, Fundamentals of turbulent gas–solid flows applied to circulating fluidized bed combustion, Progress in Energy and Combustion Science 24 (1998) 259–296.
[15] P.C. Johnson, R. Jackson, Frictional-collisional constitutive relations for granular materials, with application to plane shearing, Journal of Fluid Mechanics 176 (1987) 67–93.
[16] D.G. Schaeffer, Instability in the evolution equations describing incompressible granular flow, Journal of Differential Equations 66 (1987) 19–50.
[17] A. Darelius, A. Rasmuson, B. van Wachem, I. Niklasson Björn, S. Folestad, CFD simulation of the high shear mixing process using kinetic theory of granular flow and frictional stress models, Chemical Engineering Science 63 (2008) 2188–2197.
[18] K. Johansson, Fluid dynamics and erosion in a fluidized bed for energy production—a numerical and experimental study, PhD Thesis, Chalmers University of Technology, Sweden, 2004.
[19] S.M. Eldighidy, R.Y. Chen, R.A. Comparin, Deposition of suspension in the entrance of a channel, Journal of Fluids Engineering, Transactions of the ASME 99 (1977) 365–370.
[20] J.Y. Tu, C.A.J. Fletcher, Numerical computation of turbulent gas–solid particle flow in a 90° bend, AIChE Journal 41 (1995) 2187–2197.
[21] J. Kilander, A. Rasmuson, Energy dissipation and macro instabilities in a stirred square tank investigated using an LE PIV approach and LDA measurements, Chemical Engineering Science 60 (2005) 6844–6856.
[22] P.C. Knight, J.P.K. Seville, A.B. Wellm, T. Instone, Prediction of impeller torque in high shear powder mixers, Chemical Engineering Science 56 (2001) 4457–4471.
[23] J.D. Litster, K.P. Hapgood, J.N. Michaels, A. Sims, M. Roberts, S.K. Kameneni, Scale-up of mixer granulators for effective liquid distribution, Powder Technology 124 (2002) 272–280.
[24] J.X. Bouillard, R.W. Lyczkowski, D. Gidaspow, Porosity distributions in a fluidized bed with an immersed obstacle, AIChE Journal 35 (1989) 908–922.